doi:10.1093/brain/aws102 Brain 2012: 135; 1695–1713 | 1695

BRAIN
A JOURNAL OF NEUROLOGY

Titin mutation segregates with hereditary myopathy with early respiratory failure

Gerald Pfeffer,[1,2] Hannah R. Elliott,[1] Helen Griffin,[1] Rita Barresi,[1,3] James Miller,[4] Julie Marsh,[3] Anni Evilä,[5] Anna Vihola,[5] Peter Hackman,[5] Volker Straub,[1] David J. Dick,[4,6] Rita Horvath,[1] Mauro Santibanez-Koref,[1] Bjarne Udd[5,7,8,*] and Patrick F. Chinnery[1,4,*]

1 Institute of Genetic Medicine, Newcastle University, NE1 3BZ, UK
2 Clinician Investigator Program, University of British Columbia, Vancouver, V5Z 1M9, Canada
3 Muscle Immunoanalysis Unit, Newcastle Hospitals NHS Trust, Newcastle, NE2 4HH, UK
4 Department of Neurology, Newcastle upon Tyne Hospitals NHS Foundation Trust, NE1 4LP, UK
5 Folkhälsan Institute of Genetics and Department of Medical Genetics, Haartman Institute, University of Helsinki, Helsinki 00014, Finland
6 Department of Neurology, Norfolk and Norwich University Hospital, NR4 7UY, UK
7 Neuromuscular Research Centre, Department of Neurology, University Hospital and University of Tampere, Tampere 33520, Finland
8 Department of Neurology, Vaasa Central Hospital, Vaasa 65130, Finland

*These authors contributed equally to this work.

Correspondence to: Patrick F Chinnery,
Institute of Genetic Medicine,
Central Parkway,
Newcastle, NE1 3BZ,
UK
E-mail: patrick.chinnery@ncl.ac.uk

In 2001, we described an autosomal dominant myopathy characterized by neuromuscular ventilatory failure in ambulant patients. Here we describe the underlying genetic basis for the disorder, and we define the neuromuscular, respiratory and radiological phenotype in a study of 31 mutation carriers followed for up to 31 years. A combination of genome-wide linkage and whole exome sequencing revealed the likely causal genetic variant in the titin (*TTN*) gene (g.274375T>C; p.Cys30071Arg) within a shared haplotype of 2.93 Mbp on chromosome 2. This segregated with the phenotype in 21 individuals from the original family, nine subjects in a second family with the same highly selective pattern of muscle involvement on magnetic resonance imaging and a third familial case with a similar phenotype. Comparing the mutation carriers revealed novel features not apparent in our original report. The clinical presentation included predominant distal, proximal or respiratory muscle weakness. The age of onset was highly variable, from early adulthood, and including a mild phenotype in advanced age. Muscle weakness was earlier onset and more severe in the lower extremities in nearly all patients. Seven patients also had axial muscle weakness. Respiratory function studies demonstrated a gradual deterioration over time, reflecting the progressive nature of this condition. Cardiomyopathy was not present in any of our patients despite up to 31 years of follow-up. Magnetic resonance muscle imaging was performed in 21 affected patients and revealed characteristic abnormalities with semitendinosus involvement in 20 of 21 patients studied, including 3 patients who were presymptomatic. Diagnostic muscle histopathology most frequently revealed eosinophilic inclusions (inclusion bodies) and rimmed vacuoles, but was non-specific in a minority of patients. These findings have important clinical implications. This disease should be considered in patients with adult-onset proximal or distal myopathy and early respiratory failure, even in the presence of non-specific muscle pathology. Muscle magnetic resonance imaging findings are characteristic and should be considered as an initial investigation, and if positive

Received February 13, 2012. Revised March 6, 2012. Accepted March 7, 2012. Advance Access publication May 9, 2012

should prompt screening for mutations in *TTN*. With 363 exons, screening *TTN* presented a major challenge until recently. However, whole exome sequencing provides a reliable cost-effective approach, providing the gene of interest is adequately captured.

Keywords: hereditary myopathy with early respiratory failure; cytoplasmic body; titin; exome sequencing; distal myopathy
Abbreviations: LGMD = limb girdle muscular dystrophy

Introduction

Respiratory muscle weakness is a common late feature of many neuromuscular disorders, but usually develops after the onset of significant limb or axial weakness. Defects of neuromuscular transmission and motor neuron disease (amyotrophic lateral sclerosis) occasionally require immediate ventilation on presentation (Qureshi *et al*., 2004; Gautier *et al*., 2010), as can α-glucosidase deficiency (acid maltase deficiency, type II glycogenosis) (Mellies and Lofaso, 2009) and rare presentations of other inherited, metabolic, inflammatory or toxic myopathies (Hutchinson and Whyte, 2008). However, in general, respiratory failure is unusual in ambulant patients. In contrast, several European families have been described where affected individuals developed significant ventilatory weakness early in the disease course (Patel *et al*., 1983; Chapon *et al*., 1989; Edstrom *et al*., 1990; Abe *et al*., 1993; Chinnery *et al*., 2001; Birchall *et al*., 2005). Sporadic cases with similar clinical and pathological features have also been described (Kinoshita *et al*., 1975; Jerusalem *et al*., 1979; Winter *et al*., 1986; Bertini *et al*., 1990; Baeta *et al*., 1996; Evangelista *et al*., 2009; Tasca *et al*., 2010). Differences in the neuromuscular phenotype led to several different names for the clinical syndromes, including hereditary myopathy with early respiratory failure (OMIM #603689), hereditary cytoplasmic body myopathy with early respiratory failure (Jerusalem *et al*., 1979; Patel *et al*., 1983; Chapon *et al*., 1989; Abe *et al*., 1993), hereditary inclusion body myopathy with early respiratory failure (Chinnery *et al*., 2001) and myopathy with respiratory failure and myofibrillar aggregates (Kinoshita *et al*., 1975; Edstrom *et al*., 1990). All reported cases shared in common the presence of early respiratory muscle involvement, and predominantly proximal and/or distal muscle weakness with pathological features including eosinophilic inclusions on muscle histopathology and Z-disc abnormalities with cytoplasmic bodies on electron microscopy. A mutation in the kinase domain of titin was identified as the cause in three Swedish families (Lange *et al*., 2005), but the genetic cause of the disease in all the other patients remained elusive.

In 2001, we described a family with an autosomal dominant myopathy associated with early respiratory failure (Chinnery *et al*., 2001). The disorder presented in mid-adult life in 11 individuals with predominantly distal weakness and preferential diaphragmatic involvement in some patients. Hip and shoulder girdle weakness developed later in the disease course. The absence of axial weakness distinguished the family from other clinical descriptions, and the disease did not link to genetic loci known to be relevant at the time. Subsequent studies defined the lower-limb muscle magnetic resonance imaging (MRI) phenotype, with prominent semitendinosis and obturator externus involvement, which was detectable in clinically unaffected individuals at risk of inheriting the disorder (Birchall *et al*., 2005). Here, we report the genetic basis of this disease and confirm our clinical suspicion that two other families have the same disorder. This allowed us to define the clinical spectrum of the disease in 31 patients.

Materials and methods

Clinical assessments

Ethical approval was granted by the Newcastle University and Hospitals Local Research Ethics Committee. All assessments and clinical investigations were carried out in the Newcastle upon Tyne Hospitals NHS Foundation Trust. Clinical data were available for 31 affected individuals. A structured history and examination was performed on 22 subjects (P.F.C., R.H. and G.P.), along with routine haematological, biochemical, immunological and endocrine blood tests, including serum creatine kinase. Clinical neurophysiology (electromyography and nerve conduction studies, $n = 13$), muscle MRI ($n = 21$) and skeletal muscle biopsy ($n = 15$) were performed on a subgroup of affected individuals.

Muscle biopsy analysis

Diagnostic skeletal muscle biopsies were snap frozen on site for histopathological and histochemical examination on cryostat sections (15 biopsies) and western blot analysis (7 biopsies). Diagnostic immunocytochemistry was performed using the following commercially available antibodies. Dystrophin: Dy10/12B2 (N-terminus), Dy4/6 D3 (rod), Dy8/6C5 (C-terminus). Associated glycoproteins: Ad1/20A6 (α-sarcoglycan), βSarc1/5B1 (β-sarcoglycan), 35DAG/21B5 (γ-sarcoglycan), δSarc3/12C1 (δ-sarcoglycan), 43DAG/8D5 (β-dystroglycan). β-Spectrin: RBC2/3D5 (to monitor membrane integrity on sections). Laminins: commercial anti-laminin α5 (Chemicon MAB 1924), β1 (Chemicon MAB 1921) and γ1 chain (Chemicon MAB 1920), Mer3/22B2 (equivalent to 300 kDa α2 chain fragment) on sections; commercial α2 (Chemicon MAB 1922) (80 kDa fragment) on blots. Caveolin 3, Emerin and lamin A/C: commercial antibodies (Transduction Labs C38320 and Novocastra NCL-LAM-A/C, respectively). Calpain 3: Calp3d/2C4 (exon1), Calp3c/12A2 (exon 8) on blots only. Dysferlin: NCL-hamlet (exon 53) on blots and sections, Ham3/17B2 (at exon 11-12 junction) on sections. Telethonin (G-11), neonatal myosin heavy chain (NCL-MHCn), on sections only. Titin antibody m10-1 (Hackman *et al*., 2008) was used on western blots.

Pathological analysis of muscles from post-mortem examination

Immunohistochemistry

Post-mortem samples (quadriceps, gastrocnemius, diaphragm, cardiac) obtained from Patient A-IV:17 were analysed. Control skeletal muscle

was obtained during orthopaedic surgical intervention in individuals not suffering from neuromuscular diseases. A standard immunohistochemistry protocol was used on 6-μm frozen sections with antibodies against desmin (Dako D33, 1:400), myotilin (Novocastra NCL-Myotilin, 1:50) and P62 (Abcam ab56416, 1:150). Labelling for calpain 3 (Novocastra NCL-CALP-2C4, 1:50) and valosin-containing protein (BD Biosciences, 1:2000) was carried out with a sensitive detection protocol (X-Cell-Plus HRP Detection, Menapath) as previously described (Charlton *et al*., 2009).

Sodium dodecyl sulphate polyacrylamide gel electrophoresis and western blotting

Sections (30 × 10 μm) were cut for each sample and quickly dissolved in loading buffer (0.05 M dithiothreitol, 0.1 M EDTA, 0.125 M Tris, 4% sodium dodecyl sulphate, 10% glycerol, 0.005% bromophenol blue, pH 8), boiled for 3 min and centrifuged. Gel electrophoresis and transfer were carried out as described (Anderson *et al*., 1999). After transfer, nitrocellulose membrane sheets were labelled with monoclonal anti-calpain antibodies (Novocastra NCL-CALP-2C4 and NCL-CALP-2A12, both 1:60) that detect the full size calpain 3 at 94 kDa and degradation fragments of the protein at 60 or 30 kDa or rabbit polyclonal m10-1 at 1:500, raised against the most C-terminal titin doman M10 (Hackman *et al*., 2008). Antibody detection was performed using an enhanced chemiluminescence detection system (Thermo Scientific SuperSignal® West Pico Chemiluminescent Substrate). Proteins on gel were stained with Coomassie Brilliant Blue after transfer. Dried blots and gels were used for densitometric analysis with AlphaView™ Q Software (Alpha Innotech).

Genome-wide linkage analysis

A total of 28 individuals (of which 21 were affected) were genotyped at 1170 microsatellite markers derived from the Applied Biosciences HD Marker linkage set and deCODE designed markers derived from the Marshfield genetic map. The average marker distance was 4 cM, with 95% of the gaps <6 cM and none >10 cM. Proprietary deCODE Allele Caller software was used for automated allele calling. CEPH family DNA samples were used as quality controls. Markers (93.7%) were successfully genotyped.

Two-point and multipoint linkage analysis was performed using ALLEGRO v1.2c (incorporated into the EasyLINKAGE Plus package) (Gudbjartsson *et al*., 2000; Lindner and Hoffmann, 2005). An autosomal dominant mode of inheritance and a parametric model-based assumption with complete penetrance and a disease allele frequency of 0.1% were used for analysis.

Fine mapping

A further nine markers were used to fine-map the linked locus: two markers were proximal to D2S335 (D2S2380 and D2S399) and seven were distal to this marker (D2S2257, D2S148, D2S2173, D2S324, D2S1574E, D2S385 and D2S2310). One oligonucleotide from each pair was fluorescently labelled (sequences available on request). In addition to 50 ng DNA, 1 × GoTaq® buffer (Promega), 0.33 μM of each oligonucleotide, 2.5 mM dNTPs (Roche) and 0.5 U *Taq* polymerase (Promega) were added, to a final volume of 15 μl. Amplification was initiated by denaturation at 95°C for 2 min, followed by 30 cycles of denaturation at 95°C for 1 min, annealing at 57–61°C for 1 min and extension at 72°C for 1 min. Finally, there was a further extension at 72°C for 3 min before the samples were cooled to 4°C. Amplicons (3 μl) were utilized for downstream analysis of microsatellite sizes by using a CEQ8000™ Genetic analysis system (Beckman Coulter) according to manufacturer's instructions. Analysis was conducted using Beckman Coulter Fragment Analysis v2.2.1 software.

Array comparative genomic hybridization

Array comparative genomic hybridization was performed on an affected individual (Patient A-IV:12) by using a whole genome 4 × 44k oligo array (ISCA version 2.0), analysed with Bluefuse Multi v2.4 software, with expected resolution of ~0.25 Mb.

Whole exome sequencing and bioinformatics

Whole exome sequencing was initially performed on two subjects (Patients A-III:6 and A-IV:12) by using the Agilent SureSelect Human All Exon (38 Mb) capture system, and subsequently on another affected individual (Patient A-IV:10) by using the Illumina TruSeq™ Exome Enrichment (62 Mb) capture system. Genomic DNA was fragmented, hybridized and exonic sequences were enriched according to manufacturer's protocol. The captured DNA fragments were purified and sequenced on an Illumina Genome Analyser IIx using 75 bp reads (single and paired-end, respectively) for Patients A-III:6 and A-IV:12, and an Illumina Hiseq2000 platform using 100 bp paired-end reads for Patient A-IV:10. Sequence reads were aligned to the human reference genome (UCSC hg19) using BWA (Li and Durbin, 2010) and the aligned sequence files were reformatted using SAMtools (Li *et al*., 2009). Single base variants were identified using Varscan v2.2 (Koboldt *et al*., 2009) and indels were identified using Dindel v1.01 (Albers *et al*., 2011). The raw lists of variants were filtered using in-house Perl scripts to identify variants within target regions that were not present in dbSNP132 or in the exome sequences of 50 unrelated and unaffected individuals. Putative 'disease causing' mutations were identified using MutationTaster (Schwarz *et al*., 2010) with the intention to screen any mutations causing amino acid substitutions and/or were predicted as deleterious.

Segregation analysis

Detection of the candidate mutations was performed by direct sequencing. The details of the specific primer sequences are available in the Supplementary material. Polymerase chain reaction was performed with Immolase (Bioline) according to manufacturer's protocol, using ~50 ng of DNA, 0.25 mM of each oligonucleotide and 0.75–4 mM $MgCl_2$, for 30 cycles with annealing temperature of 57–65°C. Sequencing was performed using BigDye® (Applied Biosystems) according to the manufacturer's protocol with an ABI 3130XL sequencer. Additional single nucleotide variants flanking the disease mutation identified by exome sequencing were Sanger sequenced to further define the disease haplotype for between-family comparisons.

Analysis of titin protein expression

Western blot analysis was carried out using the rabbit polyclonal antibody m10-1 (Hackman *et al*., 2008) to the C-terminus of titin on Patient A-III:6, compared to normal control muscle and muscle from patients with tibial muscular dystrophy and LGMD2J. The titin C-terminus is fragmented, and we use the pattern and intensity of the fragments to assess the integrity of titin C-terminus.

Results

Patients

Pedigrees for the three families are represented in Fig. 1. There were no genealogical links between the three families, although all are based in the North East of England. The clinical features of all affected individuals are summarized in Table 1, and serial pulmonary function testing results are presented in Fig. 2. A key identifying previously published patients is included in Appendix A.

Family A

Originally described with 11 affected and 13 unaffected individuals (Chinnery *et al*., 2001), the family now has 21 affected and 20 unaffected individuals. The phenotype was variable within the members of this family. Age of onset varied from 33 to 71 years. The most common presenting symptom was foot drop in 5/12 patients, exertional dyspnoea and/or orthopnoea in 4/12 patients and proximal weakness in 3/12 patients. Despite the common initial presentation of distal weakness, on clinical examination we judged the myopathy to be predominantly proximal in 5/12 patients, predominantly distal in 3/12 patients and both in the remainder. Weakness was generally more severe in the lower extremities, particularly for hip flexion and ankle dorsiflexion. Weakness was symmetrical in all patients except one (Patient A-III:6), although as his condition progressed his weakness became symmetric (particularly of ankle dorsiflexion 0/5 and hip flexion 2/5). Neck flexor weakness was present in 5/12 patients. Evidence of respiratory muscle weakness was indicated by decreased forced vital capacity and forced expiratory volume in 8/12 of the patients, and when recorded pulmonary function decreased in the supine position. Five of 12 patients eventually required nocturnal non-invasive ventilatory support for respiratory muscle weakness, and in these patients this occurred between 5 and 8 years after the time of initial assessment in our clinic. One of these patients has been receiving nocturnal ventilation for 18 years and continues to live at home. Walking aids were eventually required by most of the patients in this family, most commonly ankle-foot orthoses for foot drop, which became necessary between 1 and 4 years after initial presentation. Two of 12 patients became wheelchair-bound after an interval of 7–8 years. Mild to moderate elevations of creatine kinase were present in 7/12 patients. Neurophysiology revealed myopathy with spontaneous activity in 2/5 patients, myopathic changes in 2/5 patients and was normal in one mildly affected individual.

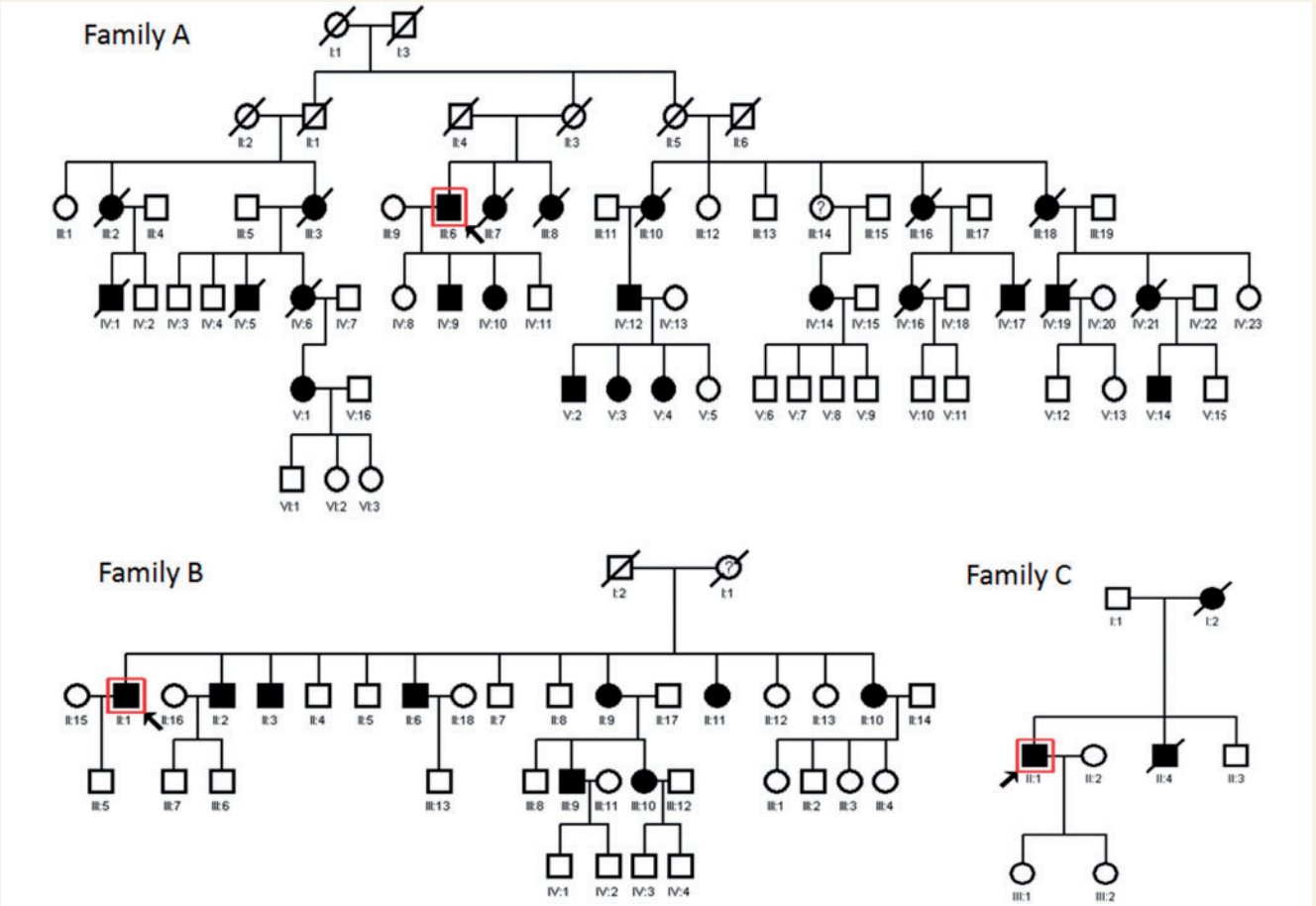

Figure 1 Pedigrees of the three families with hereditary myopathy with early respiratory failure. Part of Families A and B have been published previously (Appendix A). Surrounding box and arrow indicate the proband in each pedigree. Open symbols represent unaffected family members, filled symbols are affected by hereditary myopathy with early respiratory failure.

Table 1 Clinical features at the time of initial clinical assessment in three families (22 affected individuals)[a]

Patient ID	Onset age	Onset symptom	Proximal versus distal predominant	Weakness pattern at presentation				Pulmonary function percentage predicted		CK (u/l)[b]	NCS/EMG
				Distal	Proximal	Axial	Respiratory	FEV1	VC		
Family A											
A-III:3	71	Proximal and distal wk	Proximal = distal	ADF/APF 4	D 4+, HF 4	Normal				88	
A-III:6	47	Drop foot	Distal	ADF (R) 4-, (L) 1, AI 4-	HF (R) 4-, (L) 3, KF 4	Normal		72	68	218	
A-III:7	55	Dyspnoea	Proximal	Normal	D 4+, HF 4+	NF 4+	Symptomatic on exertion	56	62	185	
A-III:8	61	Dyspnoea	N/A	Normal	Normal	Normal	Dyspnoea, orthopnoea	73	77.5	112	Normal
A-III:16	54	Falls	Proximal = distal	FF/FE 3, WF/WE 4, ADF 4, APF 4+	D 3, EF/EE 4, HF 2, HE 3, KF/KE 4-	NF 4, NE 4+					
A-IV:4	45	Dyspnoea	N/A	Normal	Normal	Normal	Dyspnoea			77	Myopathic (proximal)
A-IV:6	48	Proximal wk	Proximal	ADF 4	D 4+, HF 3, KE 4	NF 4+	Symptomatic on exertion	107 (83 sup)	100 (80 sup)	94	
A-IV:10	38	Proximal wk	Proximal	Normal	D 4+, HF/HE 4+	Normal				327	
A-IV:12	44	Drop foot and dyspnoea	Distal	ADF 3	HF 4	Normal		40	43	237	Myopathic
A-V:14	36	Drop foot	Distal	FF/FE 4, WF/WE 4, ADF 3, AE 4	HF 4	Normal		56	67	549	Necrotizing myopathy
A-IV:16	33	Drop foot	Proximal	WE/WF 4+	D 4-, EF/EE 4, HF 3, HE 4-, ADF 4	NF 4+	Symptomatic on exertion	63	61 (53 sup)	303	Necrotizing myopathy
A-IV:20	42	Unknown	Proximal	WF 4+, ADF 4	D 4, EF/EE 4, HF 2, HE/HA 3, KF 4, KE 4-	NF 4, NE 4+		35	38		
A-V:1	22	Proximal wk and orthopnoea	Proximal	All 4	D 4-, EF/EE 4, HF 4-, HE 4	Normal				48	Normal
Family B											
B-II:1	30	Drop foot	Distal	WF 4+, ADF 3, AI 4-, AE 4, APF 5		Normal		102	92	966	Necrotizing myopathy (distal predominant)
B-II:2	44	Drop foot	Distal	ADF 4	D 4+, EE 4+, HF 4+	Normal		67	63	242	Necrotizing myopathy (distal predominant)
B-II:3	40	Drop foot	Distal	ADF/AI/AE 4-	FE/WE 4	NF 4				566	Myopathic
B-II-6	42	Drop foot	Distal	ADF 4		Normal				620	Necrotizing myopathy
B-II:9	41	Proximal wk	Proximal	ADF 4, APF 4	D 4, HF 3, HE 4, KE/KF 4	Normal		70	76	312	Necrotizing myopathy
B-II:10	45	Drop foot	Distal	FE 4+, ADF/AE/AI 3, APF 4+	HF 4+, KE 4+	NF 4					
B-II:11	55	Proximal wk and orthopnoea	Proximal = distal	ADF 4	HF 4+	Normal		66	68		
B-III:9	43	Exertional dyspnoea	Distal	ADF 4+	Normal	Normal	Symptomatic on exertion	59	66	398	Necrotizing myopathy
Family C											
C-II:1	45	Drop foot	Distal	WE/WF 4-, FE/FF 4-, ADF 2, APF 4-	EE 4+, HF 3, KE/KF 4	Normal		47	46	167	Myopathic

a All muscles not reported are MRC strength 5/5 (normal).
b The reference range for creatine kinase is 10–190 u/l at our centre.
ADF = ankle dorsiflexion; AE = ankle eversion; AI = ankle inversion; APF = ankle plantarflexion; CK = creatine kinase; D = deltoid; EE = elbow extension; EF = elbow flexion; FE = finger extension; FF = finger flexion; KE = knee extension; KF = knee flexion; HA = hip adduction; HE = hip extension; HF = hip flexion; NCS = nerve conduction studies; NE = neck extension; NF = neck flexion; sup = supine; WE = wrist extension; WF = wrist flexion; wk = weakness; FEV1 = forced expiratory volume in 1 second; VC = vital capacity; EMG = electromyography; R = right; L = left.

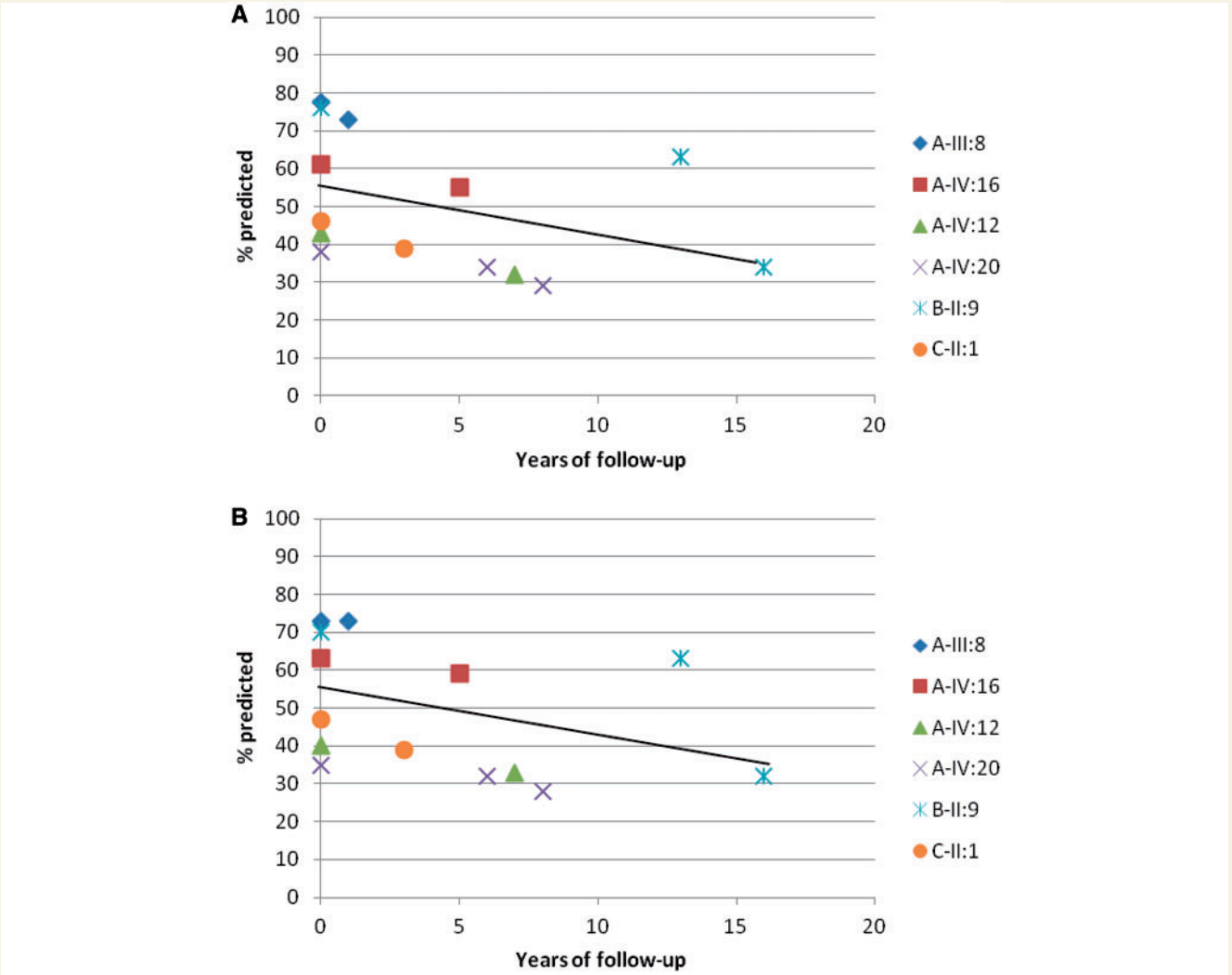

Figure 2 Pulmonary function testing results showing a gradual decline over time for (**A**) forced vital capacity and (**B**) forced expiratory volume. Results expressed as the percentage of expected values for height, gender and weight. Unique identifiers are shown for individual patients. A solid line indicates the line of best fit.

Family B

Based in a different region of the North East of England, Family B was identified on clinical grounds and shared distinctive MRI features with Family A (Birchall *et al*., 2005). Since then we have identified nine affected family members, and at present 19 family members are unaffected. Detailed clinical records were available for all nine affected family members. Age of onset varied from 22 to 55 years, and again we observed heterogeneous phenotype. Five patients presented with drop foot, three patients with symptoms of proximal weakness and three with respiratory symptoms. On clinical examination we judged that six of the patients had predominantly distal muscle involvement, particularly of ankle dorsiflexion; two of these patients had atrophy in the anterior compartment of the distal lower extremity (Patients B-II:1 and B-II:3). Mild to moderate elevations of creatine kinase were present in six patients. Neurophysiology demonstrated myopathy with spontaneous activity in 5/7 patients and was normal in one patient.

Family C

Living in the same region as Family B, the index case presented with drop foot at the age of 45 years. His mother had been wheelchair-bound since he was a child and had a diagnosis of muscular dystrophy on her death certificate. His brother had difficulty with strength in his arms and legs but died at age 47 years from unrelated causes (liver cirrhosis). On initial assessment, the proband had pronounced weakness of ankle dorsiflexion and less so of hip flexion. Calf hypertrophy was present. He also had milder grade weakness of the proximal and distal upper extremities. He was referred for ankle-foot orthoses upon our initial assessment, and became wheelchair-bound 10 years after his initial presentation. He required nocturnal continuous positive airway pressure ventilation 11 years following initial assessment. Despite having a forced vital capacity $<40\%$ for the last seven years, with nocturnal ventilation the patient has continued to live at home with assistance.

Muscle histology and protein analysis

Diagnostic muscle biopsy results from 15 subjects

We present a summary of the pathological findings from 15 affected members from all three families, which includes seven previously reported subjects (Table 2). The most common findings were eosinophilic inclusions ('inclusion bodies') and blue-rimmed vacuoles. Inclusions were found in a small minority of muscle fibres (typically <5%), even in severely affected individuals. However, affected fibres typically contained multiple inclusions. Inclusions had absent staining on NADH, succinyl dehydrogenase, periodic acid-Schiff and myophosphorylase assays, but intense staining with Gomori trichrome. Other non-specific myopathic features were variably present, including fibre size variability (up to 20-fold). Immunocytochemistry excluded known dystrophinopathies, limb-girdle muscular dystrophies (LGMD) and myofibrillar myopathies as a diagnosis. Staining of calpain 3 (*CAPN3*) was normal or mildly decreased in muscle biopsies taken from quadriceps, gastrocnemius or deltoid muscle. The reduction was more marked in muscle biopsies from tibialis anterior. Three patients had mild, non-specific abnormalities on muscle biopsy that (in the absence of the family history and later genetic testing) would not have permitted a diagnosis of hereditary myopathy with early respiratory failure. Electron microscopy was only performed on biopsies from Family A and has been reported previously (Chinnery *et al*., 2001).

Analysis of diaphragm, gastrocnemius, quadriceps and cardiac muscle from a post-mortem examination

The different muscle samples showed common pathological features of varying severity. Some degree of fibre size variation, internal nucleation, fibrosis and fat replacement was observed in all muscles analysed, but these features were more marked in the diaphragm and milder in the quadriceps. Necrosis, regeneration and inflammation were not seen. A predominant feature of the gastrocnemius was the presence of fibre fragmentation and eosinophilic inclusions, while the diaphragm was predominantly affected by fibrosis and fat replacement. Normal expression of sarcolemmal proteins such as dystrophin and components of the dystrophin glycoprotein complex had earlier been confirmed on this patient (Chinnery *et al*., 2001). To investigate the nature of the inclusions and possible myofibrillar changes secondary to the defect in titin, we stained the sections with antibodies against desmin, myotilin, p62 and valosin-containing protein (Fig. 3). In all samples, most inclusions were positive for desmin, myotilin and valosin-containing protein, while only a sub-population of fibres showed reactivity to p62, indicating that ubiquitinated multi-protein aggregates containing p-tau are present in some of the cytoplasmic bodies (Nogalska *et al*., 2009). Heart histology was normal, and protein inclusions were not observed with any of the antibodies in myocardium (Fig. 3).

Calpain 3 is a known binding partner of titin (Sorimachi *et al*., 1995), and muscle biopsies of tibial muscular dystrophy and LGMD type 2J (LGMD2J) patients show variable secondary reduction in calpain 3 (Haravuori *et al*., 2001). To investigate whether this reduction may correlate with the severity of the involvement of different muscle groups, we performed calpain 3 labelling on sections and immunoblot. In control muscle, the NCL-CALP-2C4 antibody showed diffuse cytoplasmic labelling (Charlton *et al*., 2009). Fainter labelling was detected in the patient's quadriceps, gastrocnemius and diaphragm labelled with much reduced intensity (Fig. 4). The same antibody used on western blot showed reduced calpain 3 in the quadriceps and no labelling in gastrocnemius and diaphragm. Labelling with NCL-CALP-2A12 revealed a similar reduction, although calpain 3 degradation bands at ~60 kDa were still detected in the gastrocnemius (Fig. 5A).

Table 2 Summary of muscle histopathology findings in 15 patients

Patient ID	Eosinophilic inclusions	Rimmed vacuoles	Fibre splitting/ fragmentation	Atrophy	Internal nuclei	Type I fibre predominance	Fibre size variation	Other
A-III:6	+ (minimal)		+ (minimal)	+			+	
A-III:16	++	+	++	+	++	++		
A-IV:1	++		+++	+				
A-IV:4	++	+	+	+	+	+		
A-IV:6				+	++	+++	+++	
A-IV:16	+	+	++	+++	+		++	50% replacement by fat and fibrous tissue
A-IV:17	+++	+	+++	++	++		++	
A-IV:19	+	+	+	++	+	++		
A-IV:20	+++	+	++	+	++		++	Internal nuclei fragmentation atrophy
B-II:1	+	+++	++		++		+++	Massive variation of fibre size up to 20-fold
B-II:2	+	++	+++	+++			+	
B-II-6	++	+			++			
B-II:9	+	++	++	++			++	Muscle fibre hypertrophy
B-III:9							+	Myopathic features
C-II:1				+++				End-stage muscle, mostly type 2 fibres

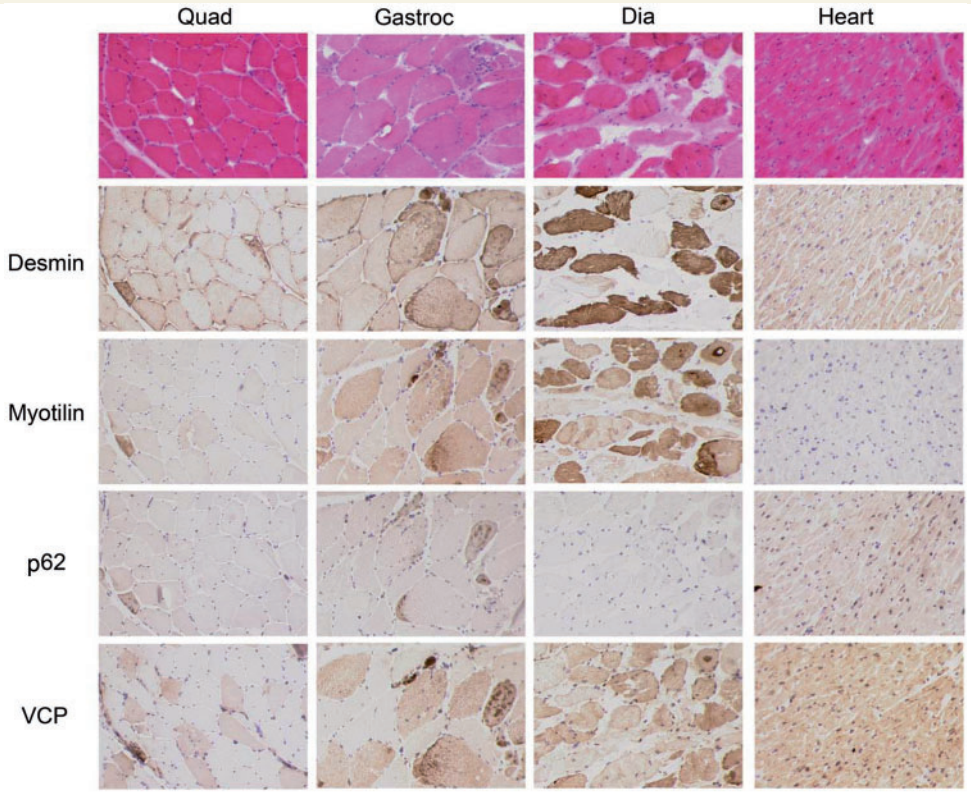

Figure 3 Post-mortem muscle pathology. Haematoxylin and eosin staining of quadriceps (quad), gastrocnemius (gastroc), diaphragm (dia) and cardiac muscle (heart) from Patient IV-12. Consecutive sections of muscles labelled with antibodies for desmin, myotilin, p62 and valosin-containing protein (VCP). The inclusions are positive for desmin, myotilin and valosin-containing protein, and some inclusions bound p62.

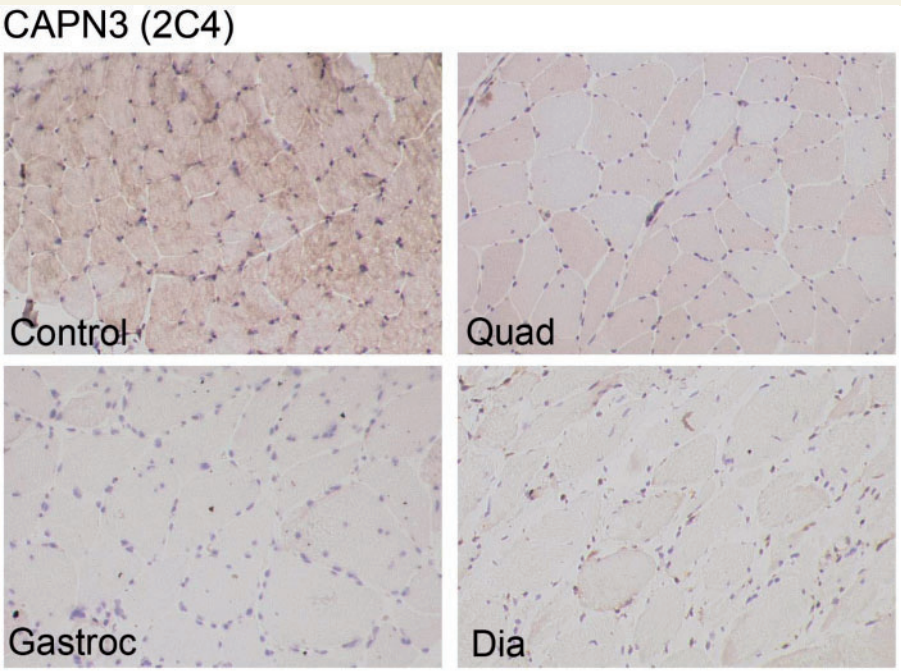

Figure 4 Calpain 3 immunocytochemistry. Control and patient muscle [quadriceps (quad), gastrocnemius (gastroc) and diaphragm (dia)] labelled with NCL-CALP-2C4 antibody against epitopes encoded by *CAPN3* exon 1. Calpain 3 expression is decreased in gastrocnemius compared with quadriceps, and not detected in diaphragm, corresponding to the severity of weakness in these muscles.

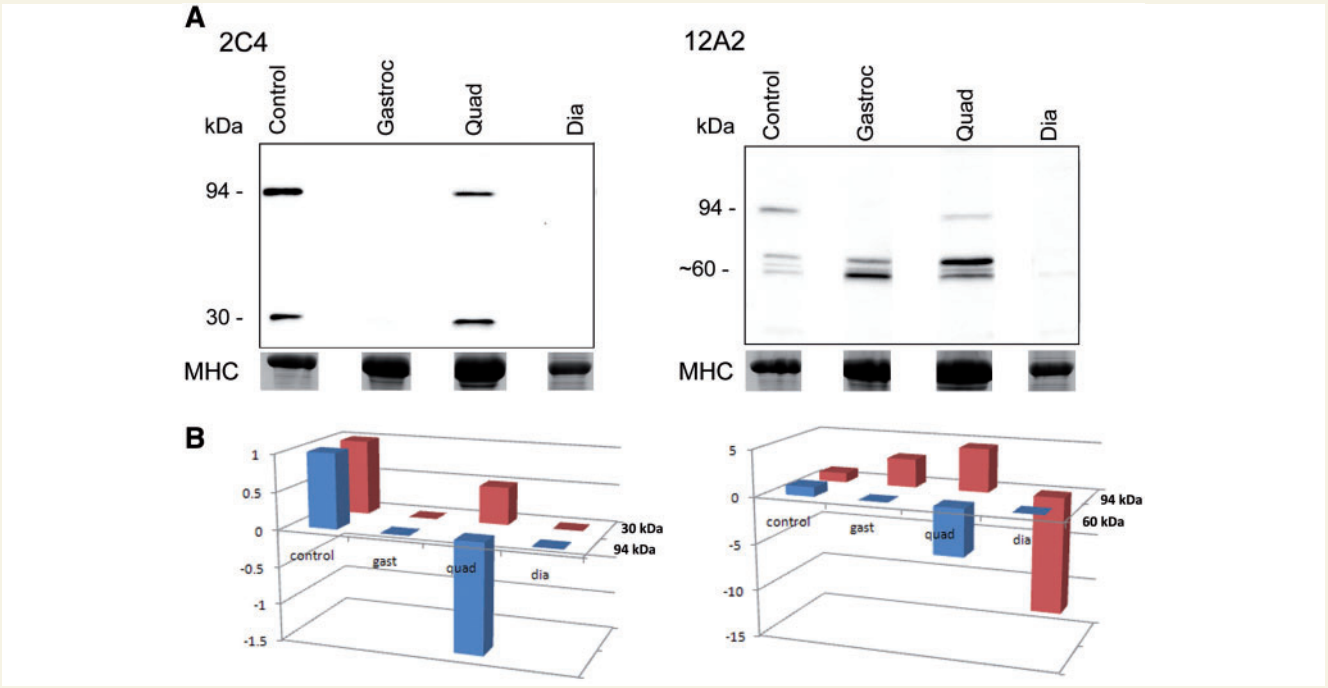

Figure 5 Western blot analysis of calpain 3. (**A**) Immunoblot of control and patient muscle samples [quadriceps (quad), gastrocnemius (gastroc) and diaphragm (dia)] labelled with NCL-CALP-2C4 and NCL-CALP-2A12 antibodies, directed against epitopes encoded by exons 1 and 8 of *CAPN3*, respectively. Myosin heavy chain (MHC) from post-blotted gel indicates the amount of protein loaded. (**B**) Densitometric analysis of calpain 3. *y*-axis = fold change in intensity.

Calpain 3 can undergo exhaustive autolysis but it is usually stable (8 h) in human muscle. When freezing or storage artefacts occur, the intensity of the 94 kDa band may be reduced on immunoblot, while an increase in abundance of degradation bands at 60 and 30 kDa is observed. Given that the samples were collected post-mortem, some degree of protein degradation should be taken into account. Indeed, densitometric data normalized to the myosin content in each lane showed that the 60-kDa degradation bands detected in quadriceps and gastrocnemius were stronger in intensity than control (Fig. 5B). Calpain 3 was not detected in the diaphragm with either antibody.

Western blot analysis of titin

Western blot analysis using an antibody directed against the M10 domain of titin showed a normal expression and banding pattern in Patient A-III:6, in contrast to patients with tibial muscular dystrophy and LGMD2J, where the C-terminal fragments were reduced or absent (Fig. 6).

Muscle magnetic resonance imaging findings

Muscle MRI findings are summarized in Table 3, and were consistent with the findings in our previous study (Birchall *et al*., 2005). Novel findings include three patients who had imaging when presymptomatic, which demonstrated similar (albeit milder) abnormalities to patients who were already clinically affected. Based on these patients, semitendinosus and peroneus longus are the first muscles to show fatty infiltration on MRI (Fig. 7).

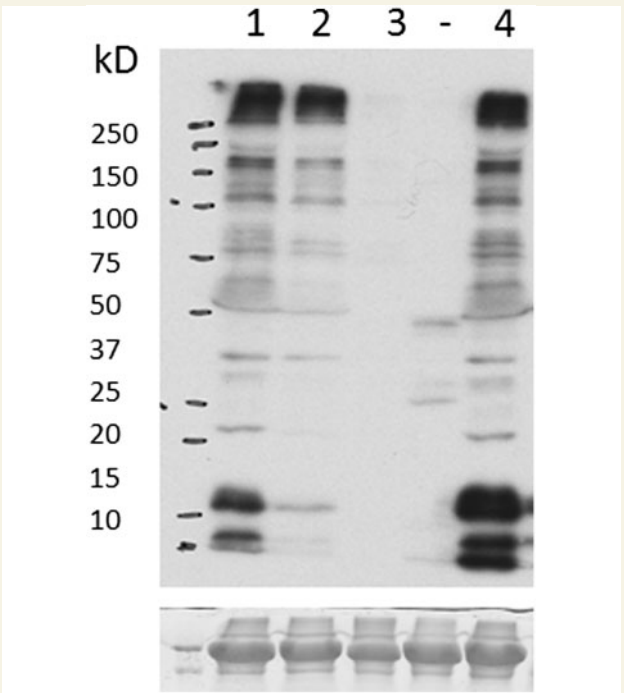

Figure 6 Western blot of the titin protein (post-blotting gel stained with Coomassie). Lane 1, healthy control muscle; Lane 2, tibial muscular dystrophy muscle; Lane 3, LGMD2J muscle; Lane (-), unrelated sample; Lane 4, quadriceps muscle from Patient A-III:6. The observed banding pattern for our patient from Family A is similar to that seen in control muscle.

Table 3 MRI findings in 21 affected patients ordered according to severity of clinical picture at time of imaging

Patient ID	Clinical status	Distal legs						Proximal legs									Axial		Upper extremities				
		PL	GS	TA	TP	EHL	EDL	ST	OE	IP	Sa	Gr	BF	Gl	SM	QF	ABD	ES	SSp	SSc	IS	D	SAn
A-IV:9	Presymptomatic	++	–	–	–	–	–	++	–	–	–	–	–	–	–	–							
A-V:3	Presymptomatic	+	–	–	–	–	–	++	+	–	++	–	–	–	–	–							
B-III:10	Presymptomatic	++	–	–	–	–	–	++	–	–	–	–	–	–	–	–							
A-V:4	Respiratory symptoms	+	–	–	–	–	–	++	+	–	+	+	–	–	–	–							
A-IV:4	Minor wk	–	–	–	–	–	–	+	–	–	–	–	+	–	–	–							
	4 year follow-up	–	–	–	–	–	–	+	–	–	–	–	+	+	+	–							
A-IV:10	Minor wk	+	+	–	–	–	+	++	++	–	++	++	–	–	–	+							
A-IV:20	Minor wk	–	–	–	–	+	–	+	–	–	–	–	–	+	–	–							
A-V:1	Minor wk	–	–	–	–	–	–	–	–	–	+	–	–	–	–	–							
A-V:2	Minor wk	++	–	++	–	–	–	+++	++	–	–	++	–	–	–	–							
B-II:2	Minor wk	+	–	+++	–	++	++	+++	++	+++	–	–	–	+	–	–	–	+	++	++	++	–	+
B-II:11	Minor wk	++	–	++	–	–	++	++	–	–	–	–	–	++	++	++							
B-III:9	Minor wk	–	–	++	–	–	++	++	++	–	–	–	–	–	–	–							
A-V:14	Moderate wk	+++	–	+++	–	–	+++	+++	++	–	++	+++	++	++	++	++							
B-II:1	Moderate wk	+++	+	+++	–	+++	+++	+++	++	+++	–	–	–	+	–	++	++	–	++	++	++	++	+
B-II-6	Moderate wk	++	++	++	–	–	++	++	++	–	–	++	–	–	–	–	–	++					
A-III:6	Severe wk	+++	++	+++	++	+++	+++	+++	+++	+++	+++	+++	–	+	–	+++	+++	–	++	–	+	–	+
A-III:7	Severe wk	–	–	–	++	–	–	+++	+++	++	–	++	–	–	–	+	++	++					
A-IV:6	Severe wk	+	–	+	–	+	–	+++	++	++	++	++	–	–	–	+	–	–	++	–	+	++	++
A-IV:12	Severe wk	++	–	++	++	++	–	+++	++	++	–	–	–	–	–	–	++	–					
B-II:3	Severe wk	+++	++	+++	++	–	+++	+++	++	–	–	–	–	–	++	+++	–	++					
B-II:9	Severe wk	+++	++	+++	+++	+	+++	+++	+++	+++	+	+++	+	++	++	+++	+++	+++	+++	++	+++	++	+++

ABD = rectus femoris and/or transversus abdominis; BF = biceps femoris; D = deltoid; EDL = extensor digitorum longus; EHL = extensor hallucis longus; ES = erector spinae; Gl = gluteals; Gr = gracilis; GS = gastrosoleus; IP = iliopsoas; IS = infraspinatus; OE = obturator externus; PL = peroneus longus; Sa = sartorius; SAn = serratus anterior; SM = semimembranosus; SSc = subscapularis; SSp = supraspinatus; ST = semitendinosus; TA = tibialis anterior; TP = tibialis posterior; wk = weakness.

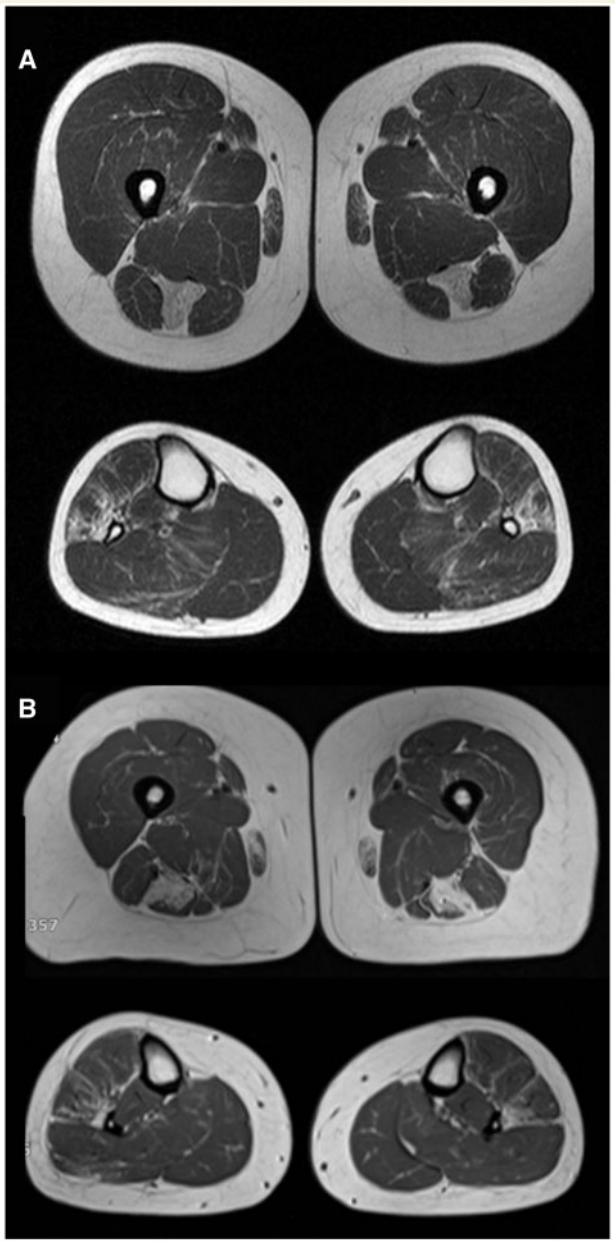

Figure 7 Muscle MRI in unaffected mutation carriers. (**A**) Patient A-IV:9 and (**B**) Patient B-III:10 in Fig. 1 remain clinically unaffected but show characteristic MRI abnormalities with symmetrical fatty replacement of semitendinosus in the proximal lower extremity, and milder involvement of peroneus longus in the distal lower extremity.

Two of these patients (Patients A-IV:9 and A-V:3) had imaging seven and six years ago, respectively (both at 30 years of age), and still have not developed the condition. The third patient (Patient B-III:10) already had mildly abnormal pulmonary function tests at the time of initial assessment and developed symptoms of muscle weakness shortly after the time of her scan.

We also report results of serial imaging in one patient (Patient A-IV:4) with a mild phenotype. She had two MRI studies in a 4-year interval showing minimal progression, in keeping with her stable clinical course over this period.

The most commonly affected muscle was semitendinosus (20 of 21 subjects), followed by peroneus longus (16/21) and obturator externus (15/21). Some of the patients with mild phenotype had mild abnormalities on imaging, although moderate and severe phenotypes were always associated with pronounced imaging abnormalities. Axial muscles were also involved, including rectus abdominis, transversus abdominis or erector spinae (total of eight patients, in advanced disease), in keeping with our observation that axial muscle weakness is common in this disorder.

Genome-wide linkage analysis

Genome-wide microsatellite analysis performed on Family A identified a 30-cM region on chromosome 2q24.1-2q32.2 with a maximum multipoint log of odds (LOD) score of 3.8 at microsatellite marker D2S335 (Fig. 8). Observed heterozygosity at this marker was 97%. No other chromosomal regions achieved multi-point LOD score of >2.0. This marker also achieved the maximum single point LOD score of 3.4. No other markers produced a single point LOD score of >2.3. Following the addition of nine further microsatellite markers surrounding D2S335, the maximum single point LOD score remained at microsatellite marker D2S335 with a LOD score of 3.8, but the maximum multipoint LOD score shifted to give a maximum LOD at marker D2S2188 located at 180.79 cM on chromosome 2. Linkage analysis and additional manual haplotype analysis within the pedigree indicated the disease locus lay between microsatellite markers D2S2188 and D2S2310, with all affected family members sharing a common haplotype flanked by these two markers. Several unaffected family members also shared the common haplotype between D2S2188 and D2S2173, indicating the disease locus was likely to be situated between markers D2S2173 and D2S2310. This represents a 3.61-cM region including titin (*TTN*).

Array comparative genomic hybridization

No abnormalities were detected with array comparative genomic hybridization.

Whole exome sequencing and bioinformatics

Whole exome sequencing using the Agilent SureSelect Human All Exon (38 Mb) capture system generated more than 152 million 75-bp paired-end reads (11.4 Gb) in Patient A-III:6 and >127 million 75-bp single-end reads (9.6 Gb) in Patient A-IV:12. The exome was captured at a mean per target base sequence depth of 111- and 116-fold for Patients A-III:6 and A-IV:12, respectively, with 88 and 91% of target bases covered at a minimum depth of 10-fold. Within the linkage region on chromosome 2, only 54 and 55% of coding exon bases (CCDS May 2009) were covered at a minimum depth of 10-fold; the coverage of *TTN* was particularly poor, with only 10% of coding bases covered at a minimum depth of 10-fold in both patients. Due to the poor coverage of *TTN*, an additional Patient A-IV:10 was sequenced using the Illumina TruSeq® Exome Enrichment (62 Mb) capture system, which

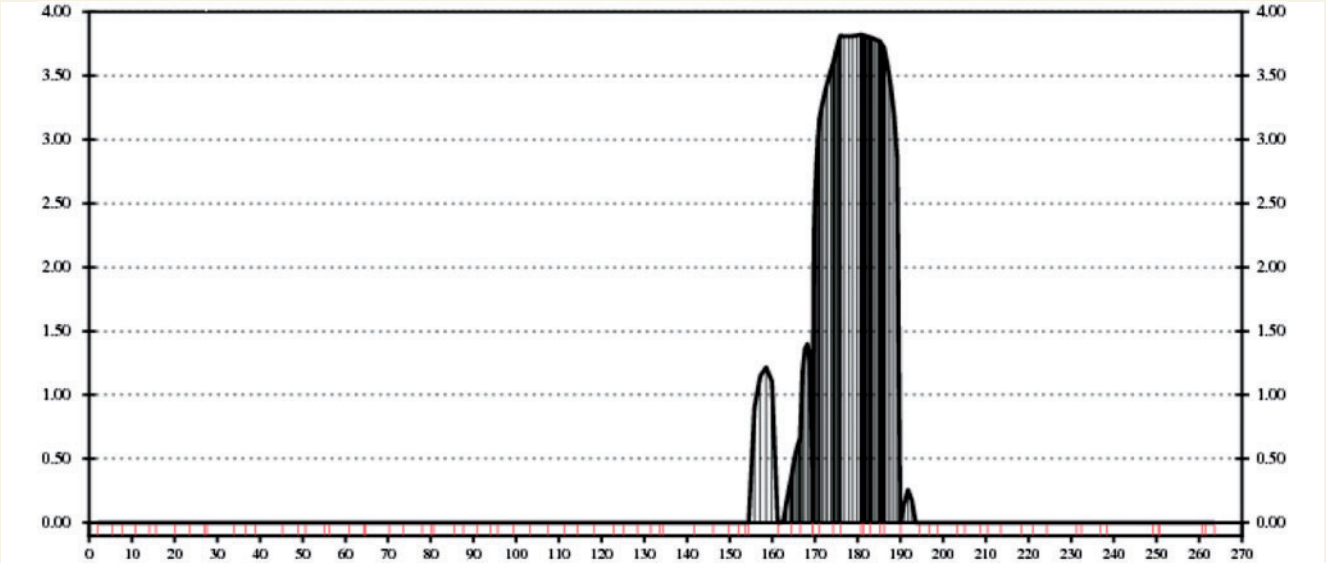

Figure 8 Multi-point linkage analysis of chromosome 2 from Families 1 and 2, using 1000 microsatellite markers, and autosomal dominant model. The linkage region of 2q24-31 includes the *TTN* gene and the haplotype, which is shared between all three families.

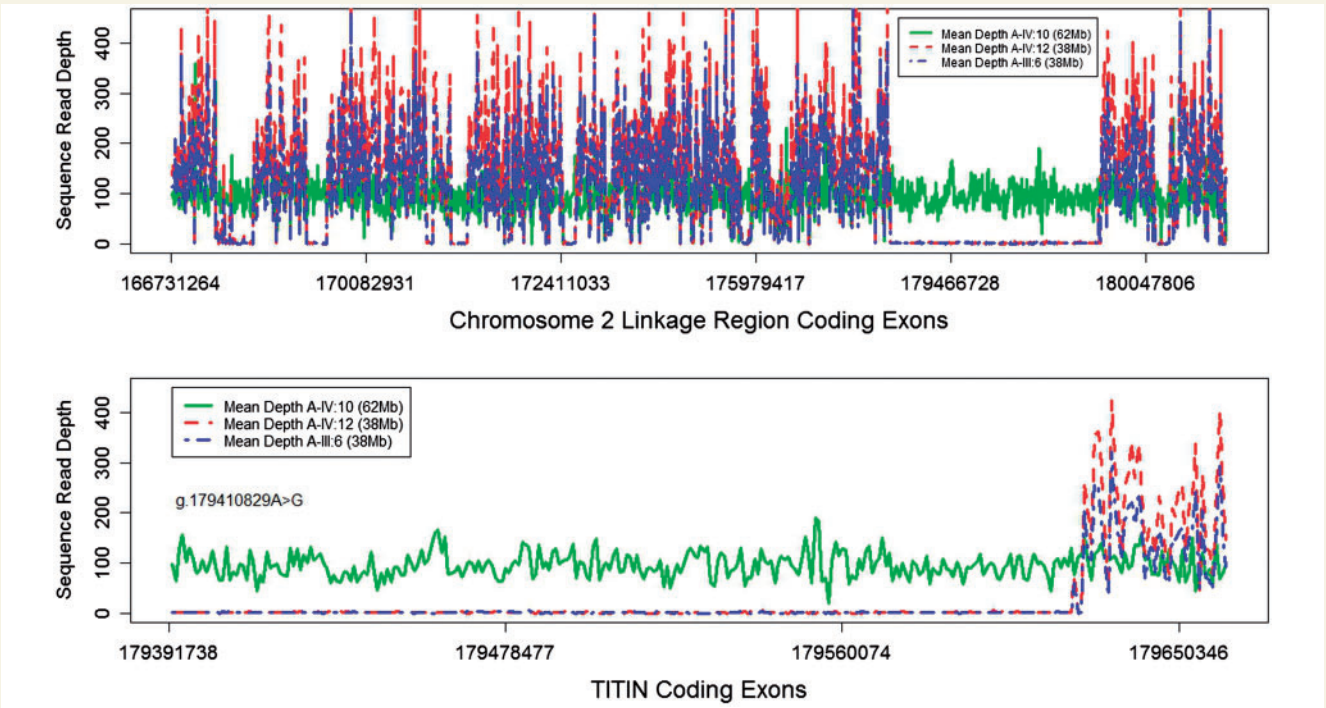

Figure 9 Whole exome sequence coverage of the linkage region in three patients. By design, the 38-Mb capture kit did not sequence the majority of the *TTN* gene (blue/red lines), although coverage was adequate for the 62-Mb capture kit (green line), thus identifying the causative mutation.

generated more than 137 million 101-bp reads (13.9 Gb). Using these targets, there was a mean per target base coverage of 99-fold and 94% of target bases were covered at a minimum depth of 10-fold. Within the linkage region, 98% of coding bases were covered (minimum 10-fold) at a mean depth of 105-fold and 99.8% of the coding region of *TTN* was covered (minimum 10-fold) with a mean depth of 105-fold. Figure 9 shows the difference in coverage between the three patients using the different exome capture systems.

Table 4 shows the number of variant predictions from the exome sequence. The initial sequencing of Patients A-III:6 and A-IV:12 yielded four novel heterozygous variants in the linkage region (Table 5: note that insertion/deletions are only available for Patient A-III:6 because a technical problem resulted in the

Table 4 Summary of genetic variants detected from the first and second whole exome sequencing runs

Patient	Variant type	Total predicted[a]	On target[b]	dbSNP132[c]	Novel[d]	Shared novel[e]	Linkage region[f]
A-IV:12	SBV	163 998	39 756	39 510	741	64	2
A-III:6		402 858	44 531	44 143	1 022		
A-IV:10		1 373 612	81 795	80 201	2 738	–	20
A-IV:12	Indel	–	–	–	–	–	–
A-III:6		104 495	2736	1571	1102	–	2
A-IV:10		56 677	9740	6683	2566	–	10

a SBV = Varscan parameters minimum total coverage ⩾ 5-fold; minimum variant coverage ⩾ 3-fold, min. Quality > 10; Indel = Dindel output filter minimum variant coverage ⩾ 4.
b Variants located within Agilent 38-Mb targets ± 500 bp (FG/AD) or Illumina 62-Mb targets ± 500 bp (RG), seen on both (forward and reverse) strands and (SBVs only) variant allele frequency > 24%.
c Variants that match dbSNP132 - hg19; there are some duplicate positions with different rs numbers included in the totals.
d Variants not found in dbSNP132.
e Novel SBVs shared between Patient A-III:6 and Patient A-IV:12.
f chr2:166 697 613–183 034 559 (reference sequence: GRCh37).

Table 5 Candidate mutations considered for segregation analysis after the first whole exome sequencing run

Gene	Chromosome	Position	Mutation type	Reference	Variant[a]	Coding change	Prediction	Segregation analysis
WIPF1	chr2	175 437 060	SBV[b]	C	T	R158K	Disease causing	Non-segregating
TTN	chr2	179 659 327	SBV[b]	G	C	Intronic	Polymorphism	Non-segregating
GORASP2	chr2	171 808 025	Deletion	T	–G	Intronic	Polymorphism	N/A
CDCA7	chr2	174 232 452	Insertion	A	+T	3′-UTR	Polymorphism	N/A

Novel heterozygous variants shared between both patients (Patients A-III:6 and A-IV:12), within the linkage region.
a All variants are reported in the forward (5′ to 3′) direction; therefore, for reverse coding genes (such as *TTN*) intragenic locations are in reverse complement to those above.
b SBV = Varscan parameters minimum total coverage ⩾ 5-fold; minimum variant coverage ⩾ 3-fold, min.

Table 6 Candidate mutations considered for segregation analysis after the second whole exome sequencing run

Gene	Chromosome	Position	Mutation type	Reference	Variant[a]	Coding change	Prediction	Segregation analysis
TTN	chr2	179 410 829	SBV[c]	A	G	C30071R	Polymorphism	Segregates with disease in all family members
TTN[b]	chr2	179 443 028	SBV[c]	T	C	Intronic	Polymorphism	Non-segregating
TTN	chr2	179 455 928	SBV[c]	G	A	P17607L	Disease causing	Non-segregating
RAPGEF4	chr2	173 686 465	Deletion	T	-AA	5′-UTR	Disease causing	Non-segregating
CERKL	chr2	182 521 804	SBV[c]	C	A	5′-UTR	Disease causing	Non-segregating

Novel heterozygous variants in Patient A-IV:10, within the linkage region, with amino acid exchanges or predicted to be disease causing.
a All variants are reported in the forward (5′ > 3′) direction, therefore for reverse coding genes (such as *TTN*) intragenic locations are in reverse complement to those above.
b This variant was not predictive to be deleterious and was non-coding, but given it was in our main candidate gene we felt it prudent to sequence this gene as well.
c SBV = Varscan parameters minimum total coverage ⩾5-fold; minimum variant coverage ⩾3-fold, min.

generation of non-paired-end reads for Patient A-IV:12). One of these variants caused an amino acid substitution, although this variant did not segregate with the disease within the families. One of the variants was in the *TTN* gene and segregation analysis was performed because of high suspicion for mutations in this gene. After exome sequencing was performed on Patient A-IV:10 by using a different probe set, 30 novel variants were identified. Three of these were in *TTN* and two further were predicted to be pathogenic (a deletion in the 5′-untranslated region of *RAPGEF4* and a single base variant in the 5′-untranslated region of *CERKL*) (Table 6). These five variants were selected for segregation analysis. The remaining 25 variants either were non-coding changes that were not predicted to alter splice sites or had been eliminated in the first round of sequencing (Supplementary Table 2).

Segregation analysis

Sanger sequencing (Fig. 10) confirmed the presence of g.274375T > C in the *TTN* gene (Genebank#: AJ277892) in all affected individuals from Family A ($n = 21$), Family B ($n = 9$) and Family C ($n = 1$). The mutation was not detected in 182 ethnically-matched control subjects (364 chromosomes) or any of the unaffected family members ($n = 9$), who were sequenced using the

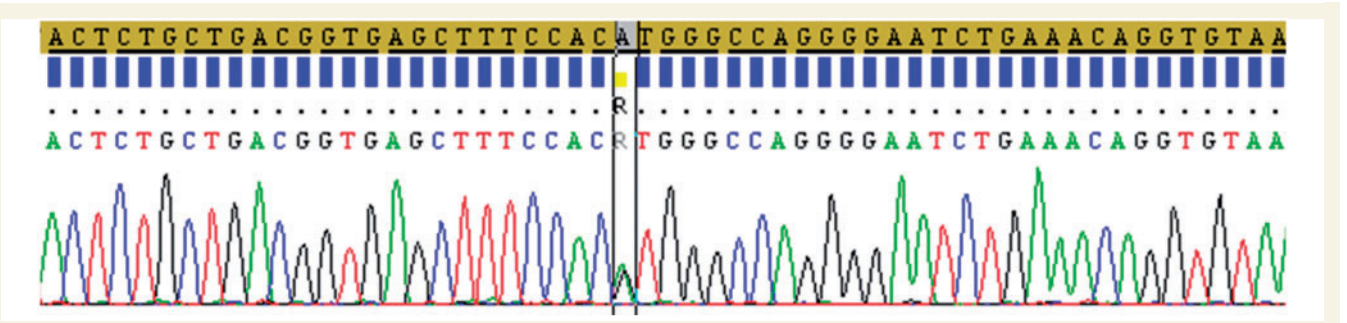

Figure 10 Confirmatory Sanger sequencing demonstrating the heterozygous g.274375T>C substitution (p.Cys30071Arg) in exon 343 of *TTN* (indicated by 'R' in the box). This approach was used for the segregation analysis in three families.

same method. Other novel variants within the linkage region that caused amino acid substitutions and/or were predicted as pathogenic by MutationTaster were sequenced using the same method and did not segregate with the phenotype. To improve our confidence that the variant was the causative mutation, we identified exons within the *TTN* gene that were covered with <10-fold read-depth. This revealed 19 regions that were sequenced using 20 primer sets and the same method above. This analysis identified heterozygous polymorphism rs116792417 and novel heterozygous intronic single base variants g.21573C>T and g.162017A>T; neither of these were predicted to cause splice site changes. Furthermore, we selected 18 single base variants from the exome sequencing of Patient A-IV:10 that were in closest proximity to the putative mutation (Supplementary Table 3). These were sequenced in the other affected family members in order to further narrow the boundaries of the shared haplotype. Two variants upstream of the putative mutation demonstrated non-sharing of alleles with the mutation. The closest was at chromosomal position 179 236 831 (using GRCh37 as the reference sequence), in which sequencing in 13 affected individuals indicated that one was homozygous for the reference allele and 12 patients had rs6433724 (eight heterozygous and four homozygous), indicating that alleles were not shared with the mutation at this location. All of the variants downstream from the mutation (the furthest being rs6715406 at position 179 650 701) were sequenced in 30 affected individuals, but it was not possible to exclude allele sharing at those locations.

These results narrowed the shared haplotype on chromosome 2 to positions 17 923 6831–182 166 459 (between rs2304340 and DS2310) for a maximum shared haplotype size of 2.93 Mb. The g.274375T>C mutation in *TTN*, which segregated with the disease in all family members, is at chromosomal position 179 410 829, which places it within this haplotype. This shared haplotype between the three families suggests a founder effect for this mutation.

Discussion

The heterozygous g.274375T>C substitution in *TTN* is highly likely to be the cause of hereditary myopathy with early respiratory failure in these families. It is a novel variant predicted to alter a highly conserved small/polar cysteine amino acid residue for a larger/basic arginine, which is likely to induce conformational change in A-band titin, and thus have functional consequences. The same variant segregates with the phenotype in three ostensibly unrelated families (a total of 31 affected and nine unaffected individuals) with the same rare disorder, and is not present in 364 control chromosomes. Other potentially pathogenic variants within the chromosomal region linked to the disease were excluded by direct sequencing. We also excluded the possibility of another mutation in *TTN* by sequencing the entire coding region of this gene. The exome sequencing had >10-fold coverage for all but 19 coding regions of *TTN*, and these remaining regions were excluded by Sanger sequencing. After further analysis of single nucleotide variants surrounding the putative mutation, the size of the shared haplotype in these three families was 2.93 Mbp, which contains only 10 protein-coding genes. The only sarcomeric protein in this region is *TTN*, and a muscle protein is the presumed cause of this disease due to the disturbed myofibrillar architecture on electron microscopy. As expected for a missense mutation, the size and abundance of the titin protein was normal in affected muscle, but the titin-binding partner calpain 3 was reduced, further implicating titin in the pathogenesis of the disorder. Finally, by carrying out a comprehensive study of the clinical phenotype in mutation carriers, we show that the clinical spectrum of disease in these families overlaps with that described in other families with mutations in the kinase domain of *TTN* (Lange, 2005), providing further evidence that *TTN* is the disease gene in the families described here.

Hereditary myopathy with early respiratory failure is a rare disease, but as we have demonstrated, there is enormous phenotypic variability within these families. The phenotype was mild or severe, with onset in early to late adulthood, and the predominant muscles affected were proximal, distal, axial, respiratory or, most frequently, a combination of these. Ultimately, nearly all patients eventually developed significant proximal and distal weakness, perhaps suggesting that the various initial presentations may converge into a common late-stage phenotype, as has been demonstrated in dysferlin myopathy (Paradas *et al*., 2010). Given these features of the condition and the difficulty in recognizing symptoms of respiratory failure due to muscle weakness (two of our patients were initially misdiagnosed as having obstructive sleep apnoea), it is quite possible that this disease is under-recognized, and the very small number of reported cases in the world literature (Table 7) may therefore under-represent the true prevalence of

Table 7 Previously reported cases of cytoplasmic body myopathy with early respiratory failure

Author, year	N	Onset age (years)	Myopathy characteristics	Other clinical features	Neurophysiology	Pathologic features	Outcome	Inheritance, linkage region
Kinoshita, 1975	1	16	Severely affected: respiratory, sternomastoid, proximal, tibialis anterior muscles Moderately affected: facial/ bulbar muscles Calf hypertrophy, areflexia, contractures	Micrognathia, cleft palate	EMG: myopathic changes	Inclusions in muscle fibre periphery. Thickened Z-discs and disorganized myofibrillar material	Death at 23 years from RF	Sporadic, N/A
Jerusalem, 1979	1	Childhood	Respiratory, axial and shoulder muscle weakness		EMG: active neurogenic changes	Numerous cytoplasmic bodies in type I fibres. Endoplasmic reticulum dilations in axons	Death at 31 years from RF	Sporadic, N/A
Patel, 1983	3	Childhood	Two patients severely affected: intercostal, sternomastoid muscles Other affected: facial and proximal muscles 1 patient: Mild proximal myopathy	Scoliosis, dysmorphic features, cardiac hypertrophy and conduction defects, constipation	EMG: myopathic changes	Cytoplasmic bodies predominant in type I fibres	14M death by RF 15F ventilator assist for respiratory infections. 55F proximal myopathy, benign course	Autosomal dominant or recessive, N/A
Winter, 1986	1	25	Respiratory and proximal muscle weakness	Polydactyly, neck stiffness	EMG: myopathic features. Diaphragmatic paralysis with phrenic nerve stimulation	Eosinophilic cytoplasmic bodies, mainly in type I fibres and internal nuclei	Requiring intermittent positive pressure ventilation at night	Sporadic, N/A
Chapon, 1989	3	18, 40, 44	Respiratory, axial and proximal weakness	Mild cardiac hypokinesis in one patient	EMG: myopathic changes.	Cytoplasmic bodies in type I fibres		Autosomal dominant, N/A
Edstrom, 1990	16 (3 families)	14–50	Respiratory, proximal and sternomastoid weakness		EMG: myopathic changes	Myofibrillar lesions in Z-disks and distributed filamentous masses. Cytoplasmic bodies		Autosomal dominant, 2q24-31, R279W *TTN* mutation (Lange, 2005)
Bertini, 1990	1	1	Respiratory failure, bulbar/ neck flexor weakness	Hyporeflexia	EMG: myopathic changes	Inclusions with positive immunostaining for desmin and actin	Death at 14 months from RF	Sporadic
Abe, 1993	5	35–48	Respiratory and distal muscle weakness, worst in tibialis anterior	Weight loss, finger contractures	EMG: myopathic changes, slight neurogenic changes	Eosinophilic inclusions. Cytoplasmic bodies predominantly in type I fibres	Early death from RF in some family members	Autosomal dominant, N/A
Baeta, 1996	1	67	Respiratory failure (limited clinical information)	Cardiomyopathy		Cytoplasmic bodies predominantly in type I fibres		Autosomal dominant, N/A
Evangelista, 2009	1	74	Hip flexor weakness, respiratory fatigue	Symptoms provoked by HMG-CoA reductase inhibitor therapy and improved with cessation	NCS: sensorimotor polyneuropathy EMG: myopathic changes, mild neurogenic changes	Eosinophilic inclusions (termed as cytoplasmic bodies but no EM analysis)	Resolution with cessation of HMG CoA reductase inhibitor	Sporadic, N/A
Tasca, 2010	1	32	Respiratory failure, neck flexor, hip flexor, hip flexor, tibialis anterior, peroneal weakness. Scapular winging and nasal voice			Eosinophilic inclusions. Diffuse IHC staining for sarcoplasmic proteins. Cytoplasmic bodies on EM. Z-line abnormalities		Sporadic, N/A (R279W *TTN* mutation was excluded)
Chinnery, 2001; Birchall, 2005; **current study**	31 (3 families)	22–71	Respiratory failure, proximal and/or distal muscle weakness, some patients with neck flexor weakness		EMG: myopathic and active neurogenic changes	Eosinophilic inclusions, some rimmed vacuoles, no fibre-type predominance. No cytoplasmic bodies on EM	Slowly progressive course. Early death from RF in one patient. Night-time CPAP and walking aids for several family members	Autosomal dominant, 2q24-31, p.Cys30071Arg *TTN* mutation

CPAP = continuous positive airway pressure; EM = electron microscopy; EMG = electromyography; IHC = immunohistochemistry; NCS = nerve conduction studies; RF = respiratory failure; M = male; F = female; HMG-CoA = 3-hydroxy-3-methyl-glutaryl-coenzyme A.

this disorder. This is compounded by the fact that muscle pathology can be non-specific (as was the case for 3/15 patients in our series), and even if detected, the presence of cytoplasmic bodies are a non-specific finding seen in other well-defined muscle diseases (Caron *et al*., 1999). Another common feature is Z-disc abnormality (Edstrom *et al*., 1990; Abe *et al*., 1993; Chinnery *et al*., 2001) and the accumulation of myofibrillar protein within inclusions, vacuoles and/or cytoplasmic bodies (Bertini *et al*., 1990; Baeta *et al*., 1996; Caron *et al*., 1999; Chinnery *et al*., 2001), which could result in cases of this disease being classified as myofibrillar myopathy [e.g. myopathy due to desmin, myotilin or filamin mutations may also present with early respiratory failure (Ferrer and Olive, 2008)]. Cytoplasmic bodies in hereditary myopathy with early respiratory failure have been found to contain desmin (Bertini *et al*., 1990; Baeta *et al*., 1996), dystrophin (Caron *et al*., 1999) and β-amyloid (Chinnery *et al*., 2001), which are also over-expressed in the muscle from patients with myofibrillar myopathy (Selcen, 2011). On account of these clinical and pathological similarities, as well as the similar genetic aetiology (since myofibrillar myopathies are caused by mutations in proteins associated with the Z-disc), it is reasonable to consider this disorder in the pathological differential diagnosis of myofibrillar myopathy, even though the hyaline and dark cytoplasmic abnormalities on trichrome stain are lacking in this disease.

By studying the largest series of patients described to date, our observations cast light on the optimal means to diagnose and manage patients with this disorder, providing a guide to the natural history. Selective fat infiltration of semitendinosus on muscle MRI was present in all but one of the patients in this series, and was also present in all presymptomatic mutation carriers before symptom onset. MRI abnormalities of semitendinosus and peroneus longus (the two most frequently affected muscles in our series) are also observed in myofibrillar myopathies, particularly desminopathy, αB-crystallinopathy and myotilinopathy (refer to diagnostic algorithm in Fig. 5 of Wattjes *et al*., 2010). These shared patterns on MRI are not likely to be coincidental: it has already been demonstrated that phenotypes resembling 'titinopathy' can be caused by mutations in αB-crystallin and that the mechanism appears to be due to altered interaction of αB-crystallin with titin protein (Inagaki *et al*., 2006; Zhu *et al*., 2009). Our series has provided MRI data on 21 patients and firmly defines the MRI features of hereditary myopathy with early respiratory failure, showing for the first time that thigh MRI is a sensitive predictor of mutation status. Future MRI algorithms should include hereditary myopathy with early respiratory failure in the category of diseases that have predominant semitendinosus and peroneal muscle involvement. This would improve recognition and appropriate genetic testing for this condition. After diagnosis, the early recognition of asymptomatic respiratory failure and its treatment with nocturnal ventilation is likely to have improved the quality and length of life, with several individuals remaining semi-independent at home up to 31 years after the initial diagnosis.

The reported cases of this disorder in the world literature are summarized in Table 7, with the majority not defined genetically. For those cases with onset in adulthood, it seems plausible that these might also be due to *TTN* mutations, given the overlap of clinical and pathological findings. One of the reported adult-onset cases had cardiomyopathy, which was not demonstrated in any of our patients. Nonetheless, titin is also expressed in cardiac muscle and it is possible a different mutation in this gene could be responsible. The massive size of titin has rendered complete screening of this gene near-impossible in the past, but exome sequencing is a cost-effective way forward. However, our findings show that this should not be considered an 'off the shelf' routine clinical test at present. Our initial exome sequencing failed to identify the causative mutation in Family A because only a small proportion of titin was sequenced following 38-Mb capture. Only by further re-sequencing using a 62-Mb capture system did we obtain adequate coverage to detect the causal variant in this family.

The spectrum of disease due to *TTN* mutations is already broad, and a schematic of the regional distribution of mutations causing the various phenotypes is summarized in Fig. 11. Mutations of the M-band region (at the C-terminal limit of the protein) cause tibial

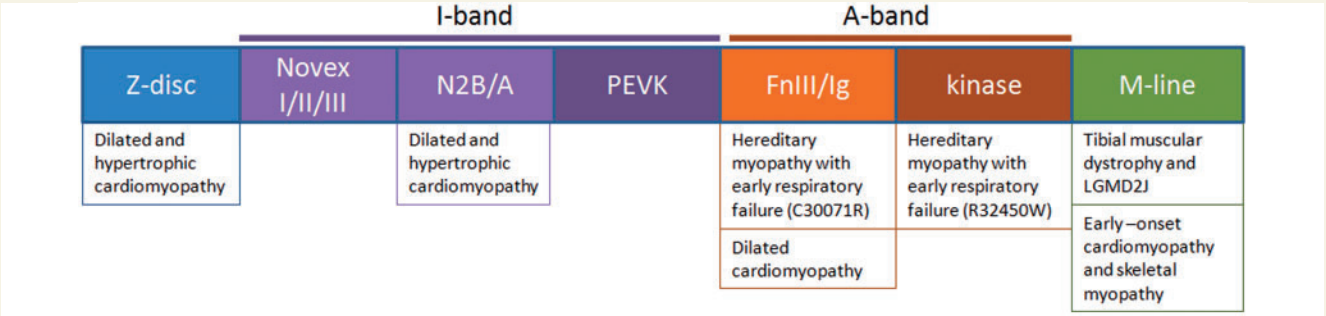

Figure 11 Schematic diagram of the various domains of *TTN* (not drawn to scale), represented from N-terminus to C-terminus, and described based on their location within the sarcomere. There is some domain specificity for the observed phenotypes. Cardiomyopathy occurs from a broad range of mutations, although those in the N2B and A-band domains are most common (Herman *et al*., 2012). Mutations causing late-onset autosomal dominant myopathies are within the A-band, kinase region and M-line: tibial muscular dystrophy is caused by mutations in the M-line, and hereditary myopathy with early respiratory failure is now demonstrated to be caused by A-band or kinase mutations. The novex and N2B regions contain isoform-specific sequences (mainly for cardiac muscle). PEVK is the region characterized by repeats of amino acids PEVK. The A-band contains repetitive fibronectin III (FnIII) and immunoglobulin-like (Ig) elements (Gregorio *et al*., 1999; Bang *et al*., 2001; Freiburg *et al*., 2000; Krüger *et al*., 2009).

muscular dystrophy in heterozygous state (Hackman *et al*., 2002), which bears some similarity to hereditary myopathy with early respiratory failure due to its onset in adulthood, and preferential involvement of ankle dorsiflexion. Mutations that cause premature stop codons have been suggested to cause a more severe phenotype of this disorder in some reported families (Hackman *et al*., 2008). M-band mutations in homozygous state cause a severe, early onset skeletal myopathy, LGMD type 2J (Udd *et al*., 2005). Homozygous deletions in the M-band are causative of early onset cardiomyopathy and skeletal myopathy (Carmignac *et al*., 2007). A missense mutation in the kinase region of *TTN* (proximal to the M-band) has been demonstrated to be causative of hereditary myopathy with early respiratory failure in three families (Lange, 2005). Interestingly, the mutation described in the current report is a missense mutation proximal to the kinase region, in the A-band of titin. This suggests that the mechanism is not directly related to altered kinase activity of titin, and further study will be required to determine the cause of early respiratory muscle involvement, which appears to be mutation-specific at present. Given the myofibrillar pathology and inclusion bodies, the mutation may cause hyperaggregation of titin and/or its binding partners in the A-band or interference with the calpain 3 proteolytic system.

Protein studies from muscle in our patients did not reveal abnormalities in the most C-terminal part of titin with the antibodies tested. However, detailed pathological studies of eight muscle biopsies and three separate skeletal muscle tissues from a single patient (post-mortem material) demonstrated decreased calpain 3 expression. Calpain 3 is a muscle-specific calcium-dependent protease responsible for LGMD2A. Secondary reduction of calpain 3 on muscle biopsies has been reported in LGMD2B (Anderson *et al*., 2000) and LGMD2I (Yamamoto *et al*., 2008), without any apparent correlation between the levels of calpain 3 and the stage of muscle pathology (Charlton *et al*., 2009). However, in the post-mortem tissue studied here, the greatly reduced levels of calpain 3 in the diaphragm correlated with the severity of the myopathy. To our knowledge, this is the first report of comparative calpain 3 analysis in multiple muscle groups from the same patient and is consistent with the role of titin as a regulatory factor controlling calpain 3 autolysis (Ono *et al*., 2006). Although preliminary, these observations suggest that secondary loss of calpain 3 may exacerbate the disease.

In conclusion, we present a detailed clinical description of the largest reported series to date of patients with hereditary myopathy with early respiratory failure. This condition has variable clinical presentation, progressive respiratory muscle weakness, occasionally highly non-specific muscle pathology and as such is likely under-recognized. We show that patients with this condition may be identified when they are presymptomatic with muscle MRI, revealing semitendinosus and peroneus longus as the first affected muscles. In more advanced cases, semitendinosus, peroneus longus and obturator externus are the most commonly affected muscles on MRI. Using microsatellite linkage analysis and whole exome sequencing, we have identified the g.274375T>C mutation in *TTN*, which lies within a 2.93-Mb haplotype shared between these three families, and excluded the possibility of another *TTN* gene mutation by sequencing all coding regions of the gene. Hereditary myopathy with early respiratory failure can be due to mutations in the A-band (as in this report) and the kinase domain, and further study will be required to discover the full repertoire of *TTN* lesions capable of causing this disease.

Acknowledgements

We are grateful to Sharon Keers for technical assistance with the linkage analysis. We thank Dr Steve Laval and Dr Hanns Lochmuller for advice relating to this research.

Funding

This work was supported by the Association Francaise Contre les Myopathies. P.F.C. is a Wellcome Trust Senior Fellow in Clinical Science and an NIHR Senior Investigator who also receives funding from the Medical Research Council (UK) through the MRC Translational Neuromuscular Centre, the Wellcome Trust Centre for Mitochondrial Research, the UK NIHR Biomedical Research Centre for Ageing and Age-related disease and Biomedical Research Unit award to the Newcastle upon Tyne Foundation Hospitals NHS Trust. R.H. is supported by the MRC (UK). G.P. receives funding from the Clinician Investigator Program (University of British Columbia) and a Bisby Fellowship from the Canadian Institutes of Health Research.

Supplementary material

Supplementary material is available at *Brain* online.

References

Abe K, Kobayashi K, Chida K, Kimura N, Kogure K. Dominantly inherited cytoplasmic body myopathy in a Japanese kindred. Tohoku J Exp Med 1993; 170: 261–72.

Albers CA, Lunter G, MacArthur DG, McVean G, Ouwehand WH, Durbin R. Dindel: accurate indel calls from short-read data. Genome Res 2011; 21: 961–73.

Anderson LV, Davison K. Multiplex Western blotting system for the analysis of muscular dystrophy proteins. Am J Pathol 1999; 154: 1017–22.

Anderson LV, Harrison RM, Pogue R, Vafiadaki E, Pollitt C, Davison K, et al. Secondary reduction in calpain 3 expression in patients with limb girdle muscular dystrophy type 2B and Miyoshi myopathy (primary dysferlinopathies). Neuromuscul Disord 2000; 10: 553–9.

Baeta AM, Figarella-Branger D, Bille-Turc F, Lepidi H, Pellissier JF. Familial desmin myopathies and cytoplasmic body myopathies. Acta Neuropathol 1996; 92: 499–510.

Bang ML, Centner T, Fornoff F, Geach AJ, Gotthardt M, McNabb M, et al. The complete gene sequence of Titin, expression of an unusual ≈700-kDa Titin isoform, and its interaction with obscurin identify a novel Z-line to I-band linking system. Circ Res 2001; 89: 1065–72.

Bertini E, Ricci E, Boldrini R, Servidei S, Fusilli S, Dionisi-Vici C, et al. Involvement of respiratory muscles in cytoplasmic body myopathy–a pathology study. Brain Dev 1990; 12: 798–806.

Birchall D, von der Hagen M, Bates D, Bushby KM, Chinnery PF. Subclinical semitendinosus and obturator externus involvement defines an autosomal dominant myopathy with early respiratory failure. Neuromuscul Disord 2005; 15: 595–600.

Carmignac V, Salih MA, Quijano-Roy S, Marchand S, Al Rayess MM, Mukhtar MM, et al. C-terminal titin deletions cause a novel early-onset myopathy with fatal cardiomyopathy. Ann Neurol 2007; 61: 340–51.

Caron A, Gohel C, Mollaret K, Morello R, Chapon F. Study of some components of the cytoskeleton in muscular disorders with nonspecific cytoplasmic bodies. Acta Neuropathol 1999; 97: 267–74.

Chapon F, Viader F, Fardeau M, Tome F, Daluzeau N, Berthelin C, et al. Familial myopathy with 'cytoplasmic body' (or 'spheroid') type inclusions, disclosed by respiratory insufficiency. Rev Neurol (Paris) 1989; 145: 460–5.

Charlton R, Henderson M, Richards J, Hudson J, Straub V, Bushby K, et al. Immunohistochemical analysis of calpain 3: advantages and limitations in diagnosing LGMD2A. Neuromuscul Disord 2009; 19: 449–57.

Chinnery PF, Johnson MA, Walls TJ, Gibson GJ, Fawcett PR, Jamieson S, et al. A novel autosomal dominant distal myopathy with early respiratory failure: clinico-pathologic characteristics and exclusion of linkage to candidate genetic loci. Ann Neurol 2001; 49: 443–52.

Edstrom L, Thornell LE, Albo J, Landin S, Samuelsson M. Myopathy with respiratory failure and typical myofibrillar lesions. J Neurol Sci 1990; 96: 211–28.

Evangelista T, Ferro J, Pereira P, de Carvalho M. A case of asymptomatic cytoplasmic body myopathy revealed by sinvastatin. Neuromuscul Disord 2009; 19: 66–68.

Ferrer I, Olive M. Molecular pathology of myofibrillar myopathies. Expert Rev Mol Med 2008; 10: e25.

Freiburg A, Trombitas K, Hell W, Cazorla O, Fougerousse F, Centner T, et al. Series of exon-skipping events in the elastic spring region of titin as the structural basis for myofibrillar elastic diversity. Circ Res 2000; 86: 1114–21.

Gautier G, Verschueren A, Monnier A, Attarian S, Salort-Campana E, Pouget J. ALS with respiratory onset: clinical features and effects of non-invasive ventilation on the prognosis. Amyotroph Lateral Scler 2010; 11: 379–82.

Gregorio CC, Granzier H, Sorimachi H, Labeit S. Muscle assembly: a titanic achievement? Curr Opin Cell Biol 1999; 11: 18–25.

Gudbjartsson DF, Jonasson K, Frigge ML, Kong A. Allegro, a new computer program for multipoint linkage analysis. Nat Genet 2000; 25: 12–13.

Hackman P, Vihola A, Haravuori H, Marchand S, Sarparanta J, De Seze J, et al. Tibial muscular dystrophy is a titinopathy caused by mutations in TTN, the gene encoding the giant skeletal-muscle protein titin. Am J Hum Genet 2002; 71: 492–500.

Hackman P, Marchand S, Sarparanta J, Vihola A, Penisson-Besnier I, Eymard B, et al. Truncating mutations in C-terminal titin may cause more severe tibial muscular dystrophy (TMD). Neuromuscul Disord 2008; 18: 922–8.

Haravuori H, Vihola A, Straub V, Auranen M, Richard I, Marchand S, et al. Secondary calpain3 deficiency in 2q-linked muscular dystrophy: titin is the candidate gene. Neurology 2001; 56: 869–77.

Herman DS, Lam L, Taylor MR, Wang L, Teekakirikul P, Christodoulou D, et al. Truncations of titin causing dilated cardiomyopathy. N Engl J Med 2012; 366: 619–28.

Hutchinson D, Whyte K. Neuromuscular disease and respiratory failure. Pract Neurol 2008; 8: 229–37.

Inagaki N, Hayashi T, Arimura T, Koga Y, Takahashi M, Shibata H, et al. Alpha B-crystallin mutation in dilated cardiomyopathy. Biochem Biophys Res Commun 2006; 342: 379–86.

Jerusalem F, Ludin H, Bischoff A, Hartmann G. Cytoplasmic body neuromyopathy presenting as respiratory failure and weight loss. J Neurol Sci 1979; 41: 1–9.

Kinoshita M, Satoyoshi E, Suzuki Y. Atypical myopathy with myofibrillar aggregates. Arch Neurol 1975; 32: 417–20.

Koboldt DC, Chen K, Wylie T, Larson DE, McLellan MD, Mardis ER, et al. VarScan: variant detection in massively parallel sequencing of individual and pooled samples. Bioinformatics 2009; 25: 2283–5.

Krüger M, Linke WA. Titin-based mechanical signalling in normal and failing myocardium. J Mol Cell Cardiol 2009; 46: 490–8.

Lange S, Xiang F, Yakovenko A, Vihola A, Hackman P, Rostkova E, et al. The kinase domain of titin controls muscle gene expression and protein turnover. Science 2005; 308: 1599–1603.

Li H, Durbin R. Fast and accurate long-read alignment with Burrows-Wheeler transform. Bioinformatics 2010; 26: 589–95.

Li H, Handsaker B, Wysoker A, Fennell T, Ruan J, Homer N, et al. The sequence alignment/map format and SAMtools. Bioinformatics 2009; 25: 2078–9.

Lindner TH, Hoffmann K. easyLINKAGE: a PERL script for easy and automated two-/multi-point linkage analyses. Bioinformatics 2005; 21: 405–7.

Mellies U, Lofaso F. Pompe disease: a neuromuscular disease with respiratory muscle involvement. Respir Med 2009; 103: 477–84.

Nicolao P, Xiang F, Gunnarsson LG, Giometto B, Edstrom L, Anvret M, et al. Autosomal dominant myopathy with proximal weakness and early respiratory muscle involvement maps to chromosome 2q. Am J Hum Genet 1999; 64: 788–92.

Nogalska A, Terracciano C, D'Agostino C, King Engel W, Askanas V. p62/SQSTM1 is overexpressed and prominently accumulated in inclusions of sporadic inclusion-body myositis muscle fibers, and can help differentiating it from polymyositis and dermatomyositis. Acta Neuropathol 2009; 118: 407–13.

Ono Y, Torii F, Ojima K, Doi N, Yoshioka K, Kawabata Y, et al. Suppressed disassembly of autolyzing p94/CAPN3 by N2A connectin/titin in a genetic reporter system. J Biol Chem 2006; 281: 18519–31.

Paradas C, Llauger J, Diaz-Manera J, Rojas-Garcia R, De Luna N, Iturriaga C, et al. Redefining dysferlinopathy phenotypes based on clinical findings and muscle imaging studies. Neurology 2010; 75: 316–23.

Patel H, Berry K, MacLeod P, Dunn HG. Cytoplasmic body myopathy. Report on a family and review of the literature. J Neurol Sci 1983; 60: 281–92.

Qureshi AI, Choundry MA, Mohammad Y, Chua HC, Yahia AM, Ulatowski JA, et al. Respiratory failure as a first presentation of myasthenia gravis. Med Sci Monit 2004; 10: CR684–9.

Schwarz JM, Rodelsperger C, Schuelke M, Seelow D. MutationTaster evaluates disease-causing potential of sequence alterations. Nat Methods 2010; 7: 575–6.

Selcen D. Myofibrillar myopathies. Neuromuscul Disord 2011; 21: 161–71.

Sorimachi H, Kinbara K, Kimura S, Takahashi M, Ishiura S, Sasagawa N, et al. Muscle-specific calpain, p94, responsible for limb girdle muscular dystrophy type 2A, associates with connectin through IS2, a p94-specific sequence. J Biol Chem 1995; 270: 31158–62.

Tasca G, Mirabella M, Broccolini A, Monforte M, Sabatelli M, Biscione GL, et al. An Italian case of hereditary myopathy with early respiratory failure (HMERF) not associated with the titin kinase domain R279W mutation. Neuromuscul Disord 2010; 20: 730–4.

Udd B, Vihola A, Sarparanta J, Richard I, Hackman P. Titinopathies and extension of the M-line mutation phenotype beyond distal myopathy and LGMD2J. Neurology 2005; 64: 636–42.

Winter JH, Neilly JB, Henderson AF, Stevenson RD, Doyle D, Wiles CM, et al. Life-threatening respiratory failure due to a previously undescribed myopathy. Q J Med 1986; 61: 1171–8.

Wattjes MP, Kley RA, Fischer D. Neuromuscular imaging in inherited muscle diseases. Eur Radiol 2010; 20: 2447–60.

Yamamoto LU, Velloso FJ, Lima BL, Fogaca LL, de Paula F, Vieira NM, et al. Muscle protein alterations in LGMD2I patients with different mutations in the Fukutin-related protein gene. J Histochem Cytochem 2008; 56: 995–1001.

Zhu Y, Bogomolovas J, Labeit S, Granzier H. Single molecule force spectroscopy of the cardiac titin N2B element: effects of the molecular chaperone alphaB-crystallin with disease-causing mutations. J Biol Chem 2009; 284: 13914–23.

Appendix A

Current study	Birchall, 2005	Chinnery, 2001
Family A		
Patient A-III:2		Patient III:3
Patient A-III:3		
Patient A-III:6	Patient A1	Patient III:15
Patient A-III:7	Patient A2	Patient III:11
Patient A-III:8		
Patient A-III:16		Patient III:10
Patient A-IV:1		Patient IV:1
Patient A-IV:4		
Patient A-IV:6	Patient A3	
Patient A-IV:9		
Patient A-IV:10		
Patient A-IV:12	Patient A4	Patient IV:3
Patient A-V:14		
Patient A-IV:16		Patient IV:15
Patient A-IV:17		Patient IV:12
Patient A-IV:19		Patient IV:7
Patient A-IV:20	Patient A5	Patient IV:11
Patient A-V:1		
Patient A-V:2		
Patient A-V:3		
Patient A-V:4		
Family B		
Patient B-II:1	Patient B3	
Patient B-II:2	Patient B2	
Patient B-II:3		
Patient B-II-6		
Patient B-II:9	Patient B1	
Patient B-II:10		
Patient B-II:11		
Patient B-III:9		
Patient B-III:10		
Family C		
Patient C-II:1		